Egress-enhancing mutation reveals inefficiency of non-enveloped virus cell exit

Valerie J. Rodriguez-Irizarry[1], Robert W. Maples[1], Julie K. Pfeiffer[1]*

[1] Department of Microbiology, University of Texas Southwestern Medical Center, Dallas, TX 75390

*Corresponding Author: Julie K. Pfeiffer
Email: Julie.Pfeiffer@UTSouthwestern.edu

Keywords: Murine norovirus; Egress; Non-enveloped virus; Evolution

Abstract

Viruses encounter a range of selective pressures, but inefficiencies during replication can be masked. To uncover factors that limit viral replication, we used forward genetics to enrich for a murine norovirus (MNV) mutant with faster replication. We sequentially harvested the earliest progeny in cultured cells and identified a single amino acid change in the viral NS3 protein, K40R, that was sufficient to enhance replication speed. We found that the NS3-K40R virus induced earlier cell death and viral egress compared with wild-type virus. Mechanistically, NS3-K40R protein disrupted membranes more efficiently than wild-type NS3 protein, potentially contributing to increased mitochondrial dysfunction and cell death. Mice infected with NS3-K40R virus had increased titers, suggesting that increasing egress did not reduce fitness *in vivo*. Overall, by using a forward genetic approach, we identified a previously unknown inefficiency in norovirus egress and provide new insights into selective pressures that influence viral replication and evolution.

Introduction

Viral replication is a complex process and exposure to selective pressures can drive viral adaptation [1-3]. In particular, RNA viruses are highly adaptable due to the high mutation rates of RNA-dependent RNA polymerases, which lack proofreading [2, 4-7]. Adaptive mutations can enhance viral replication under various selective pressures, including neutralizing antibodies [8], replication within animals [9], and heat exposure [10]. Forward genetic screening has revealed viral adaptive changes and illuminated unexpected replication defects. For example, in a previous study, we demonstrated that a mutation in the capsid of coxsackievirus B3 (CVB3) increased replication in cultured cells by destabilizing the virion and facilitating more efficient viral RNA release during uncoating [11]. Therefore, viral adaptive mutations can reveal new insights into unanticipated facets of viral replication.

Murine norovirus (MNV), a nonenveloped positive single-stranded RNA virus from the *Caliciviridae* family, serves as a model enteric virus [12, 13]. The MNV genome is approximately 7.4 kb and encodes three to four open reading frames (ORFs) [12, 14]. Translation of ORF1 produces a polyprotein that is cleaved by the viral protease to generate the mature non-structural proteins NS1–7 [14]. The viral RNA replication complex has been linked to vesicular clusters [15, 16] and includes the RNA-dependent RNA polymerase (RdRp) (NS7), VPg (NS5), and nucleoside triphosphatase (NTPase)/RNA helicase (NS3)[17]. MNV lab strains share 87% or greater genetic identity [18] and can cause either acute (MNV1 CW3) or persistent infections (MNV3, MNV CR6, MNV CR3) in mice [19, 20]. In cell culture, MNV replicates efficiently in dendritic and macrophage cell lines [21], and many groups use immortalized macrophage cell lines, such as BV2 and RAW264.7, for MNV studies. Replication kinetics can vary, but capsid proteins are detectable as early as 6 hours post-infection and progeny virions are typically observed 9 to 12 hours after infection [21]. Therefore, the 12-24 hour timeframe is frequently used for *in vitro* infection experiments.

NS3 is a multifunctional protein essential at different stages of replication. The NS3 C-terminal domain contains the evolutionarily conserved viral helicase and NTPase, both of which are required for viral genome replication [22, 23]. Caliciviruses induce cell death [24-30], and previous studies have implicated NS3 in this process[31, 32].Recently, it was demonstrated that the N-terminal region of NS3 promotes viral egress [31, 32]. Wang et al. showed that NS3 interacts with mitochondrial lipids, including cardiolipin, and disrupts cardiolipin-containing liposomes, leading to mitochondrial dysfunction and subsequent cell death [31, 33]. Notably, in the absence of this NS3-mediated cell death function, infected cells accumulate large numbers of progeny viruses that fail to exit and spread. However, the large 158 amino acid domain deletion in NS3 in that study makes it difficult to disentangle effects on egress from other facets of replication.

In this study, we selected for MNV mutants with enhanced replication speed by sequentially harvesting the earliest progeny, at 6 hours post-infection, in cultured cells. We found that a single amino acid change in the viral NS3 protein was sufficient to enhance replication. The NS3-K40R mutant induced earlier cell death and viral egress compared to wild-type MNV. Furthermore, the NS3-K40R mutant virus had increased titers in mice. Our findings suggest that viruses can adapt to selective pressures to accelerate replication, and forward genetic approaches are valuable tools for uncovering unanticipated factors that influence viral replication.

Results

Forward Genetic Screen for Fast-Replicating MNV Mutants.

To determine whether MNV could adapt to replicate more rapidly, we performed serial passage of MNV3 in BV2 cells, harvesting the early progeny. MNV progeny can be detected at high titers after 12 hours post-infection [21, 34]. For serial passage, we infected BV2 cells with MNV3 at an MOI 0.1 and we collected combined cells and culture supernatants for each sample at two different time points: 6 hours post-infection to harvest the earliest progeny, or 24 hours post-infection to harvest progeny from a complete replication cycle. The low-yield virus collected at 6 hours was amplified in BV2 cells overnight to achieve higher titers. Samples were then freeze-thawed to release intracellular virus, and half of the sample was used for a new passage. This process was repeated for 11 passages (Figure 1A). After 11 passages, we performed a viral infection assay for 6 hours at an MOI 0.1 to determine the phenotype of the passaged virus compared to the input stock. Samples collected at 6 hours post-infection (Passage 11-6 hrs) produced higher yields than the input stock virus (Passage 0) or samples collected at 24 hours post-infection (Passage 11-24 hrs) (Figure 1B). We also performed a single-cycle growth curve to determine replication kinetics and observed higher viral titers from Passage 11-6 hrs compared to Passage 0 at early time points of infection (Figure 1C). For example, passage 11-6 hrs virus had 42-fold higher titers at 8 hours post-infection compared with Passage 0 virus. These data suggest that the passaged virus (Passage 11-6 hrs) produced progeny viruses earlier than Passage 0 virus.

A Single Mutation, NS3-K40R, Is Sufficient for the Fast-Replication Phenotype.

We performed consensus sequencing to determine whether mutations contributed to the increased replication kinetics of the Passage 11-6 hrs virus. Viral genomes from Passage 11-6 hrs and Passage 11-24 hrs were amplified using RT-PCR and products were sequenced. We identified a total of three mutations in Passage 11-6 hrs virus, at nucleotides 1147, 2047, and 7022 (Figure 2A). The mutation at nucleotide 2047 resulted in an amino acid substitution from isoleucine to threonine (I340T) in non-structural protein 3 (NS3), which was present in both Passage 11-6 hrs and Passage 11-24 hrs. Given that I340T was present in both selective (Passage 11-6 hrs) and non-selective (Passage 11-24 hrs) conditions, it is possible that this mutation is due to drift or general cell culture adaptation. Indeed, we recently identified a mutation at this site, I340V, in MNV genomes following adaptation to replication in HeLa cells [35]. On the other hand, two mutations were unique to the viral progeny from Passage 11-6 hrs: a missense mutation nucleotide 1147 that resulted in substitution from lysine to arginine (K40R) in NS3 and a silent mutation at nucleotide 7022 in the minor capsid protein VP2 (A114).

To determine if the NS3-K40R or VP2-A114 mutations were sufficient to increase replication kinetics, we cloned them into an MNV3 infectious clone plasmid using site-directed mutagenesis and generated virus stocks. We infected BV2 cells at MOI 0.1, collected combined cells and supernatant for each sample at 4, 6, and 8 hours post-infection, and viral titer was determined via plaque assay. NS3-K40R showed higher viral titers, most notably at 8 hours post-infection, with ~5-fold higher titers than cells infected with WT (Figure 2B). The titers from VP2 A114 were similar to WT. These data suggest that NS3-K40R was sufficient to confer increased replication kinetics. To assess when the NS3-K40R mutation arose during passaging, we performed consensus sequence analysis for progeny from previous passages, focusing on the NS3 N-terminal region. Mutation of adenine to guanine (A<u>A</u>G to A<u>G</u>G), which confers the NS3-K40R substitution, was first observed at Passage 4, and predominated the population by Passage 8 (Figure 2C).

NS3 is a multifunctional protein with enzymatic activity in the viral replication complex [22, 23] and a role in cell death and viral egress [31, 32]. MNV NS3 protein has three domains: the N-terminal domain (amino acids 1–158), the core domain (amino acids 158–289), and the C-terminal domain (amino acids 290–364) [22, 31]. Specifically, the NS3-K40R mutation is in the N-terminal domain of NS3. Lysine at position 40 is conserved among murine noroviruses (Figure 2D, highlighted in yellow); however, it is less conserved among other members of the *Caliciviridae* family. For example, human norovirus has arginine and Tulane virus has glutamine at this position (Figure 2D). These data suggest that the impact of this region of NS3 may vary across the *Caliciviridae* family.

NS3-K40R Does Not Alter RNA Synthesis or NTPase activity.

To determine whether NS3-K40R enhances replication kinetics through effects on RNA replication and/or its enzymatic functions, we quantified viral RNA accumulation in infected cells and NTPase activity of purified proteins. First, we quantified viral genome copy numbers early in infection. BV2 cells were infected at an MOI 2, harvested at 2, 4, and 6 hours post-infection, and viral RNA was quantified by qRT-PCR. No differences in genome copies were observed between NS3-K40R and WT virus (Figure 3A). Second, to evaluate NTPase activity, we purified NS3 proteins and measured ATP hydrolysis via release of inorganic phosphate [23]. We expressed NS3 as maltose-binding protein (MBP) fusion proteins and purified full-length His6-MBP-NS3 WT and K40R using affinity chromatography. To ensure equal protein concentrations for the NTPase assay, purified proteins and an MBP control were analyzed by SDS-PAGE and band intensities were quantified (Figure 3B). Then, WT or NS3-K40R proteins were incubated with ATP for 30 minutes at 37°C, and phosphate release was measured using a colorimetric assay. ATP was efficiently hydrolyzed by MBP-NS3, confirming its NTPase activity. However, no differences in ATP hydrolysis were observed between WT and K40R. As a control, MBP alone did not show detectable phosphate release (Figure 3C). These data demonstrate that NS3-K40R does not alter genome copy numbers during infection or ATP hydrolysis of purified protein, suggesting that the mutation does not enhance RNA synthesis.

NS3-K40R Enhances Viral Egress.

Given that NS3-K40R did not alter RNA synthesis, we examined a later stage in the replication cycle, viral release/egress. As a non-enveloped virus, MNV progeny are fully assembled intracellularly prior to release. To examine egress, BV2 cells were infected at an MOI 0.1 and viral progeny were collected at 4, 6, and 8 hours post-infection from two distinct sites: cell-associated progeny within cells vs. extracellular progeny in the media. Plaque assays revealed no differences in the viral titers of cell-associated virus between NS3-K40R and WT-infected cells, further supporting the idea that NS3-K40R does not alter RNA synthesis or earlier replication stages (Figure 4A). However, NS3-K40R virus had increased extracellular viral titers compared with WT, including a ~7-fold increase in viral yield at 8 hours post-infection (Figure 4B). To determine whether effects extend to cell lines other than BV2 cells, we quantified extracellular viral yield of WT vs. NS3-K40R in RAW264.7 macrophages. We found increased viral yield of NS3-K40R virus in the supernatant of RAW264.7 cells after 8 hours post-infection (Supplemental Figure 1), suggesting that NS3-K40R facilitates earlier viral egress in multiple cell lines.

NS3-K40R Enhances Cell Death and Membrane Disruption.

How does NS3-K40R induce earlier viral egress? Given that the K40R mutation is within the N-terminal domain of NS3 that induces cell death by targeting mitochondria [31], we examined cell death and production of mitochondrial reactive oxygen species both late in infection and at early time points. First, to determine whether NS3-K40R affects cell viability, BV2 cells were infected with either WT or NS3-K40R virus at MOI 2, and cell viability was measured at 6, 8, or 24 hours post-infection. At 24 hours post-infection, cell viability was reduced for both WT and NS3-K40R compared with mock infected cells. However, NS3-K40R virus induced greater cell death than WT virus (Supplemental Figure 2A). Given that NS3-K40R promotes earlier viral egress at 6 and 8 hours post-infection (Figure 4B), we next examined its effect on cell death at these early time points. As expected, cell death was minimal this early in infection. However, NS3-K40R virus induced increased cell death at 6 and 8 hours post-infection compared with WT virus (Figure 5A). Next, to assess mitochondrial damage, cells were infected as above but incubated with MitoSOX and quantified by flow cytometry to measure mitochondrial reactive oxygen species (ROS). Mirroring the cell viability results, at 24 hours post-infection, both WT and NS3-K40R infected cells had higher mitochondrial superoxide than mock infected cells, but NS3-K40R virus induced higher levels than WT virus (Supplemental Figure 2A). At 6 and 8 hours post-infection, mitochondrial superoxide levels were low, but NS3-K40R virus induced increased mitochondrial superoxide compared with WT virus (Figure 5B). These findings suggest that NS3-K40R promotes both cell death and mitochondrial disruption earlier in infection compared to WT virus.

NS3 protein binds cardiolipin [31], a phospholipid primarily localized in the inner membrane of mitochondria but that is translocated to the outer membrane during cellular stress such as infection [36-38]. To investigate whether NS3-K40R induces cell death by disrupting mitochondria, we tested its ability to disrupt

cardiolipin liposomes. Due to potential confounding effects from the His6-MBP tag on NS3 proteins for these liposome-based experiments, we cleaved the tag, purified NS3 proteins via size-exclusion chromatography, and collected predicted monomers (~39 kDa) (Supplemental Figure 3A). We then incubated varying concentrations of proteins with or without cardiolipin liposomes encapsulating terbium (III) cation (Tb^{3+}) and quantified membrane disruption through release of Tb^{3+}. As expected, there was minimal Tb^{3+} release in control experiments using BSA with liposomes or NS3-K40R in the absence of liposomes (Supplemental Figure 3B). At high NS3 protein concentration (0.5 μM), WT and K40R proteins showed no differences in their ability to disrupt cardiolipin liposomes (Supplemental Figure 3C). However, at lower concentrations (0.05 μM and 0.005 μM), NS3-K40R was still able to disrupt cardiolipin liposomes, whereas NS3 WT was not (Figure 5C). Cardiolipin membrane disruption by NS3-WT required high protein concentrations (0.5 μM or 0.1 μM) (Figure 5D). These results suggest that NS3-K40R can disrupt cardiolipin membranes at protein concentrations 10-100-fold lower than WT NS3. Overall, these data indicate that the K40R mutation enhances the ability of NS3 to target cardiolipin-containing membranes, potentially contributing to mitochondrial dysfunction and cell death.

NS3-K40R has Increased Viral Replication in *Stat1*$^{-/-}$ Mice.

To determine whether NS3-K40R alters MNV replication or pathogenesis *in vivo*, we perorally infected *Stat1*$^{-/-}$ mice with 10^6 PFU of MNV3 WT or NS3-K40R. We chose to use immunodeficient *Stat1*$^{-/-}$ mice for these experiments because MNV can induce clinical signs and even death, whereas MNV infection is generally not severe in immunocompetent mice [39, 40]. First, we monitored weight loss and clinical signs of infection. Mice were euthanized when they had lost 25% of their body weight or exhibited any critical clinical signs. In NS3-K40R-infected mice, clinical signs such as eye discharge appeared as early as 4 days post-infection. Both WT- and NS3-K40R-infected mice displayed similar clinical signs, including constipation, eye discharge, paralysis, and lethargy. Throughout the infection, NS3-K40R did not cause significant differences in weight loss or survival (Figure 6A-B). Second, we repeated the experiment but sacrificed mice at 24 hours post-infection for titer analysis via plaque assays [41]. NS3-K40R-infected mice had increased viral titers in the spleen, duodenum, ileum and colon (Figure 6C-F). Overall, the increased titers of NS3-K40R in *Stat1*$^{-/-}$ mice suggest that this mutation enhances viral replication early in infection within an immunocompromised host.

Discussion

While much is known about factors that influence viral replication, masked inefficiencies may exist that can be discovered using the power of forward genetic screens. Here, found that MNV egress can be enhanced by a mutation in NS3. This mutant virus had increased egress via enhanced cell death (Figure 4A-B, Figure 5A). More specifically, the NS3-K40R protein disrupted membranes with mitochondrial lipids more efficiently than WT protein (Figure 5C-D). NS3-K40R virus also had increased titers in *Stat1*$^{-/-}$ mice (Figure 6C-F). Overall, these results revealed a previously unknown inefficiency in calicivirus replication and reveal new insights into mechanisms of non-enveloped viral egress.

Although mutation of norovirus NS3 at position 40 has not been described previously, other mutations in NS3 have been characterized [22, 34, 35, 42]. For example, targeted mutations in the predicted phosphate-binding loop (K168Q) reduced NS3's enzymatic activities, reducing inorganic phosphate release or unwinding activity [22, 42]. Arias *et al*. identified rare variants containing NS3-T91A in mice persistently infected with MNV3 [34], and we previously identified NS3-I340V among a large number of mutations in MNV1 variants with increased replication in HeLa cells [35]. In this study, we identified an NS3 mutation with no differences in enzymatic activity but instead facilitated earlier cell death and viral egress.

Recent studies have suggested a role for the N-terminus of NS3 in cell death induction, and our results extend and elevate the importance of NS3-mediated egress *in vitro* and *in vivo* [31, 32, 43, 44]. Aktepe *et al.* demonstrated that amino acids 67–100 of NS3 induce host translation shutoff and cell death. Wang *et al.* demonstrated that N-terminal NS3 amino acids 1–158 were necessary and sufficient to induce mitochondrial dysfunction and cell death [31]. Viral genomes lacking the N-terminal domain of NS3 were capable of RNA replication and forming progeny virions, but lack of cell death and egress meant they were unable to spread, form plaques, or produce progeny in mice [31]. However, the large deletion in NS3 makes it difficult to

differentiate effects on egress from other aspects of viral replication and fitness. Here, we used an unbiased approach to enrich for faster replicating mutants and found a single conservative amino acid change in the N-terminal domain of NS3 increased egress by enhancing membrane damage, mitochondrial dysfunction, and cell death (Figure 5B-D). Thus, in a system where any mutation in the genome that increases early progeny production could be selected, the fact that an egress-enhancing mutation emerged highlights the importance and relevance of NS3-mediated MNV egress. Overall, our study cements a key role for the NS3 N-terminal region, particularly position 40, in mitochondrial membrane disruption, cell death, and MNV egress.

How does a conservative amino acid change from lysine to arginine at position 40 of MNV NS3 alter mitochondrial membrane disruption, mitochondrial dysfunction, and cell death? Previous work suggests that the N-terminal domain of MNV NS3 contains a mitochondrial localization signal, and a four-helix bundle homologous to the membrane-disruption domain of the host mixed lineage kinase domain-like (MLKL) cell death protein [22, 31, 45, 46]. For MLKL, phosphorylation triggers a conformational change that results in association with the plasma membrane, followed by membrane permeabilization via the four-helix bundle domain [46-48]. For NS3, Wang *et al*. suggest that the mitochondrial localization signal in amino acids 1-20 of NS3 directs the protein to mitochondria followed by membrane disruption via four-helix bundle domain in amino acids 25-158. Although lysine to arginine is a conserved amino acid change, there is precedent for profound functional differences for proteins that bind and alter membranes. Previous studies have shown that replacing arginine with lysine reduces the membrane translocation efficiency of peptides like Penetratin [49]. In contrast, substituting lysine for arginine enhances cellular uptake of HIV Tat protein [50]. Notably, we found that NS3-K40R protein disrupts cardiolipin-containing membranes at concentrations 10-100-fold lower than wild-type NS3 protein. Additionally, we routinely purified more NS3-K40R protein compared with NS3-WT protein, with ~3 to 6 times more NS3-K40R than WT in eight independent protein preparations (see Supplementary Figure 2A for an example). The properties of arginine and its guanidinium group in NS3-K40R may influence protein stability and interactions with membrane lipids, ultimately leading to mitochondrial disruption and cell death.

Here we show that NS3-K40R MNV3 produces progeny faster *in vitro* and replicates to higher titers in *Stat1*$^{-/-}$ mice—so why does wild-type MNV3 contain lysine rather than arginine at position 40? In general, MNV strains contain lysine at this position (Figure 2D). However, a few caliciviruses have arginine at this position, including human norovirus (Norwalk strain), Newbury-1 virus, and Turkey calicivirus. The relative egress efficiencies of these other viruses are unknown, but it is possible that other amino acids in the N-terminal region of NS3 also impact cell death and egress. Additionally, it is possible that NS3-K40R reduces fitness in some aspect of MNV3 replication, thus maintaining lysine at this position. For example, early cell death and egress of progeny may reduce viral yield in the long run—a cell that dies early may contain fewer progeny viruses than a live cell that continues to support logarithmic viral replication for hours. However, the viral replication curve for our pool of faster viruses suggests no defect in viral yields later in infection (Figure 1C). Another possibility is that early release of progeny induces early host immune responses that would then limit replication. Finally, a major determinant of viral fitness is interhost transmission. It is possible that variants with enhanced egress have reduced transmission. In the end, subtle fitness costs for NS3-K40R MNV3, or fitness costs not studied here may explain maintenance of lysine at this position. Overall, this study illuminates the importance of NS3-mediated egress of MNV and provides new insights into viral evolution and fitness.

Methods

Cells and Viruses

BV2 and RAW264.7 cells were maintained in Dulbecco's Modified Eagle Medium (DMEM) supplemented with 10% fetal bovine serum (FBS), 1% HEPES, and 1% penicillin-streptomycin. MNV3 P6 clone (Courtesy of Stephanie Karst Lab KC792553.1 [34]). Viruses were generated by transfecting HEK293T cells with infectious clone plasmids, followed by two rounds of amplification in BV2 cells to produce high-titer viral stocks. Stocks were stored at −80°C.

Viral passaging experiments

BV2 cells were seeded at 1.2 × 10^6 cells/well in 6-well plates and infected with MNV3 at an MOI 0.1. After 1 hour at 37°C, the supernatant was removed, cells were washed, and fresh media was added. Infection was continued for 6 or 24 hours before scraping cells into the media to collect pooled intracellular and extracellular progeny. Samples were freeze-thawed three times to release intracellular virus, and half of the sample was used to initiate the next infection. Low yield 6 hour passaged samples were used to infect new BV2 cells in overnight amplifications to facilitate the next passages. Passages 2-5 were performed at unknown MOI. Viral titers were determined by plaque assay after passage 5. Passaging continued with an initial MOI 0.1 for passage 6, followed by additional passages of unknown MOI. These forward genetic experiments with MNV were performed under BSL2 conditions, as approved by the UT Southwestern Institutional Biosafety Committee.

Sequencing and Cloning

We performed consensus sequencing on Passage 11 viral populations as previously described [35]. Briefly, Passage 11 viruses were used to infect BV2 cells, viral RNA was isolated at 18 hours post-infection using TRIzol reagent, and cDNA was generated by RT-PCR with SuperScript IV reverse transcriptase (ThermoFisher) using Primer X (Table 1). PCR products were made using primer sets from Table 1 and purified with the Nucleospin Gel and PCR Clean-up kit (Macherey-Nagel). Sequencing was performed by Azenta/Genewiz with the primers listed in Table 1. The sequences of the passaged viruses were compared with the sequence of initial stock (Passage 0) in SnapGene to identify mutations. We identified three mutations in Passage 11-6 hour virus: A to G at nt 1147 (NS3-K40R), U to C at nt 2047 (NS3-I340T) and C to U at nt 7022 (a silent mutation in VP2 amino acid 114). The Passage 11-24 hr samples also contained the NS3-I340T mutation, but not the NS3-K40R or silent mutation in VP2.

To determine at which passage lysine was substituted with arginine at NS3 amino acid 40, we analyzed the nucleotide sequences at position 1147. We analyzed the consensus sequence across all viral progeny passages at 6 hours using Primer set II from Table 1. The peak heights of all four nucleotides (A, G, C, T) at position 1147 were determined from the sequencing chromatogram. The percentages presented in Figure 2C were calculated based on the relative abundance of each nucleotide.

Table 1. Primers covering the MNV genome.

	Forward (5' → 3')	**Reverse** (5' → 3')
I	GT GAA ATG AGG ATG GCA ACG	G GGT CCA AAA GAT GTC AAA GA
II	G CTC AAC ATT CTC AAC ATC G	GAC CGC CTC CAG GTT GAC
III	GAC AGG ATT GAG AAC AAG GG	GTA ATC ATC AAT GGA GTA CTT G
IV	CAT GGA TAC ACC TAC CGT GA	CTG GAA CTC CAG AGC CTC AA
V	C ACC TGG GTT GTG ATT GGG	AT GTG GTA CCT GAA ATT GGC
VI	GCC AAC AAC ATG TAT GAG ATG	AGT CCT GTA ATA CTT TTC ACC A
VII	ACG CTG CAG GGC ATC TCC	CG ACC ATC CGG TAG ATG GT
VIII	T GGT CTC TGG CCG CCT TC	CTT CCC ACA GAG GCC AAT TG
IX	A CAC CGC TGA CGC CGC AG	AG CAG TAA GCA GAA ATC ATT TTC
X		TT TTA AAA TGC ATC TAA ATA CTA CT

Mutations unique to the Passage 11-6 hr samples (NS3-K40R or VP2 silent mutation) were introduced into the MNV3 plasmid using site-directed mutagenesis (Genewiz/Azenta Life Sciences). Whole-plasmid sequencing (Plasmidsaurus) confirmed the presence of the mutations of interest and absence of other

mutations. NS3-K40R and VP2-A114 viruses were generated from plasmids as described above. The presence of the mutations in the resulting viral stocks was sequence confirmed in RT-PCR products by Genewiz/Azenta Life Sciences.

Phylogenetic analysis

We analyzed the conservation of amino acids at positions 25 to 49 of NS3 in relation to the MNV3 P6 clone. Sequence data were obtained from the NCBI database, with accession numbers and related information provided in Table 2. Representative sequences for caliciviruses were selected from the International Committee on Taxonomy of Viruses (ICTV) for each genus. Amino acid sequences were analyzed and aligned using MUSCLE, and the alignments were visualized with Geneious Prime.

Table 2. List of accession numbers from Caliciviruses used for conservation analysis.

Calicivirus	General name used Figure 2E	Accession	Amino acid Accession no.
MNV1 CW3	Murine norovirus	EF014462.1	ABJ98943.1
MNV3 P6 clone	Murine norovirus	KC792553.1	AGO61997.1
MNV CR6	Murine norovirus	JQ237823.1	AEY83582.1
Norwalk virus	Human norovirus	M87661.2	AAB50465.1
Bavaria virus	Chicken norovirus	HQ010042	ADN88287
Lagovirus	Rabbit hemorrhagic disease virus	M67473	AAA47285.1
Minovirus	Fathead minnow calicivirus	KX371097	AQM56929.1
Nacovirus	Turkey calicivirus	JQ347522	AFH89833.1
Nebovirus	Newbury-1 virus	DQ013304	AAY60849.1
Recovirus	Tulane virus	EU391643	ACB38131.1
Sapovirus	Sapporovirus	HM002617	ADG03646.1
Valovirus	Saint Valerian virus	FJ355928	ACQ44559.1
Vesivirus	Feline calicivirus	M86379	AAA79326.1

Viral infection assays

Plaque assays were performed as described previously. Briefly, virus was diluted in PBS+ (PBS supplemented with 100 µg/mL $CaCl_2$ and $MgCl_2$) and incubated with BV2 cells for 20–30 minutes at 37°C for attachment. Cells were then overlaid with 1.5% methylcellulose in MEM containing 10% FBS, 1% penicillin-streptomycin, and 1% HEPES. Overlays were removed after 72 hours [35, 51].

For infection experiments and single cycle replication experiments, 1.2×10^6 BV2 cells/well in 6-well plates were infected at MOI 0.1, and at 1 hr post-infection inoculum was aspirated, cells were washed, and fresh media was added. At each timepoint, cells and supernatant were pooled from each well and collected. Samples were subject to freeze-thaw cycles three times to release any intracellular virus, and viral titers were determined by plaque assay. For experiments in Figure 4 comparing cell-associated virus vs. extracellular virus, infections were performed as above except that media were collected as the source of extracellular virus (with an additional spin to remove any floating cells) and remaining cells were washed prior to collection as the source of the cell-associated virus.

To quantify viral RNA during infection we used qRT-PCR as previously described [51]. Briefly, 6×10^6 BV2 cells were infected with MNV3 WT and NS3-K40R virus at MOI 2 followed by removal of inoculum and washing at 1 hr post-infection. At 2, 4, and 6 hrs post-infection, cells and supernatant were pooled and RNA was isolated using TRIzol. cDNA was generated, and TaqMan quantitative PCR (qPCR) for MNV was performed in triplicate for each sample as described previously to quantify viral genomes [51]. The primers used for all samples are specified in Table 3. MNV3 plasmid that had been linearized with EcoRI was used as a standard.

Table 3. List of previously published primers used for qPCR [51].

Forward Primer (5'→ 3')	GTGCGCAACACAGAGAAACG
Reverse Primer (5' → 3')	CGGGCTGAGCTTCCTGC
Probe	[6-FAM]-CTAGTGTCTCCTTTGGAGCACCTA-[BHQ1]

Protein purification

WT and NS3-K40R NS3 proteins were purified from *E. coli* using a pMAL-c6T-His6-MBP vector as previously described [31]. Briefly, protein expression was induced overnight at 20°C with 0.25 mM isopropyl β-D-1-thiogalactopyranoside after A_{600} reached 0.8-0.9. The proteins were affinity-purified by Ni-NTA agarose (Qiagen). To remove heat-shock proteins we did ATP wash that included incubation for 5 min with 20 mM Tris-HCl, 300 mM NaCl and 5mM ATP. Bound proteins were washed three times and eluted with buffer containing 20 mM Tris-HCl (pH 8.0), 300 mM NaCl, 1 mM TCEP and Imidazole 250 mM. The proteins were subsequently affinity-purified with amylose resin (NEB) and eluted with buffer containing 20 mM Tris-HCl (pH 8.0), 300 mM NaCl, 1 mM TCEP and 10 mM maltose. After purification, proteins concentration were determined and normalized using 4–20% SDS-PAGE with Coomassie Blue staining. BSA was used as the standard, and total protein intensity was quantified with ImageJ. For NTPase experiments, we used His6-MBP tagged versions of WT or K40R NS3 proteins. However, for liposome leakage assays, we used preparations of these proteins without tags. The His6-MBP tag was removed by overnight TEV digestion at 16 °C and further purified with Ni-NTA agarose. We performed dialysis to exchange media buffer A (20 mM HEPES (pH 7.5) and 150 mM NaCl). Then, TEV-cleaved NS3 proteins were purified by Superdex 200 gel-filtration column (GE Healthcare), and the predicted monomers (~39 kDa) were collected. Previous studies have demonstrated the early aggregation of NS3 during collection [23, 31]. Therefore, for liposome leakage assays, we focused on investigating the effect of NS3 as a monomer (Supplemental Figure 2A).

NTPase assay

NTPase activity of NS3 proteins was measured using Phosphate Assay Kit - PiColorLock™ (Abcam). His6-MBP-NS3-WT or His6-MBP-NS3-K40R proteins, or a MBP alone control, at 2 uM were incubated with 10 μM ATP for 30 min at 37°C, and inorganic phosphate released from ATP hydrolysis was quantified by measuring the absorbance using Biotek Synergy LX.

Cell death and mitochondrial disruption assays

Cell death was determined by measuring the levels of the nucleic acid stain Sytox (ThermoFisher) and mitochondrial reactive oxygen species were determined by measuring the mitochondria-specific superoxide indicator MitoSox Red (ThermoFisher). For both assays, 2 x 10^5 BV2 cells were infected with WT or NS3-K40R viruses at MOI 2, inocula were removed and cells washed at 1 hr post-infection, fresh media was added, and at 6 or 8 hours post-infection the relevant assay was performed. To measure cell death, BV2 cells were collected and stained with Sytox for 15 min at RT. To measure mitochondrial ROS production, BV2 cells were collected and stained with the mitochondria-specific superoxide indicator MitoSox Red for 30 min at 37°C. Cells were washed with phosphate-buffered saline (PBS) and fluorescence was quantified using a Stratedigm benchtop flow cytometer. The percentage of cells was determined using FlowJo software. The values presented in Figure 5A-B were calculated by subtracting the values of mock-treated cells from infected cells. This subtraction represents the percentage of positive cells in each condition (% positive cells=% infected cells - % mock-treated cells).

For cell viability assays, cells were infected as described above and number of live cells was determined by measuring ATP levels using the CellTiter-Glo Luminescent Cell Viability Assay (Promega) according to the manufacturer's instructions. ATP levels were measured via luminescence using a Synergy LX plate reader.

Liposome preparation and liposome leakage assay

Cardiolipin liposomes were prepared as described by Wang *et al* [31]. Briefly, lipids were obtained from Avanti Polar Lipids Inc. To prepare Tb^{3+}-encapsulated liposomes, lipids 80% POPC (1-palmitoyl-2-oleoyl-

glycero-3-phosphocholine) and 20% cardiolipin were mixed in a glass vial. Dry lipid films were obtained by evaporating under a stream of air and then hydrated at room temperature with vortex in 300 µl buffer B (20 mM HEPES (pH 7.5), 100 mM NaCl, 50 mM sodium citrate and 15 mM $TbCl_3$). Liposomes were generated by extrusion of the hydrated lipids through 100 nm polycarbonate filter (Whatman) 30 times using a Mini-Extruder device (Avanti Polar Lipids). The Tb^{3+} ions outside the liposome were removed by washing with buffer A (20 mM HEPES (pH 7.5) and 150 mM NaCl) on a centrifugal column (Amico Ultra-4, 100 K MWCO, Millipore). The liposomes were resuspended in buffer A and were stored at 4 °C and used within 24 hours.

For liposome leakage assays, 0.1 mM of Tb^{3+}-encapsulated liposomes were suspended in 250 µl buffer C (20 mM HEPES (pH 7.5) 150 mM NaCl and 50 µM of DPA) and NS3 or control proteins were added. Fluorescence of Tb^{3+} was monitored over time on a PTI spectrofluorometer using λ_{Ex}=490 nm and λ_{Em}=276 nm. At the end of the incubation, 1% Triton X-100 was added to measure complete release of Tb^{3+}.

Mouse infections

A mix of male and female *Stat1*$^{-/-}$ C57BL/6 mice between 6–8 weeks of age were obtained from Jackson Laboratories (Jax#012606) and were single-housed and left to acclimate for 5-7 days. Mice were perorally inoculated with 25 µl of 10^6 PFU MNV3 WT or NS3-K40R in DMEM with 5% FBS. At 24 hours post-infection, mice were euthanized, and tissues were collected. The tissues were homogenized by bead beating as previously described [35] and viral titers were determined via plaque assay using BV2 cells.

For survival curve and weight loss experiments we used *Stat1*$^{-/-}$ C57BL/6 mice that were bred and maintained in the UT Southwestern specific pathogen-free animal care facility. After peroral infection as described above the mice were observed and weighed for 8 days post-infection. Mice with clinical signs of disease (lost 25% body weight and/or were lethargic, had eye discharge, or paralysis) were euthanized by CO_2. The remaining mice were euthanized at the end of the study.

All animals were handled according to the Guide for the Care of Laboratory Animals of the NIH. All mouse studies were performed at UT Southwestern (Animal Welfare Assurance no. a3472-01) using protocols approved by the local Institutional Animal Care and Use Committee in a manner designed to minimize pain, and any animals that exhibited severe disease were euthanized immediately with isoflurane or CO_2.

Statistical Analysis

All error bars represent the standard error of the mean (SEM). Specific statistical test used for each experiment is indicated in the figure legends. For all pairwise comparisons, a *P*-value < 0.05 was considered significant and represented with a single asterisk. GraphPad Prism was used to perform all statistical analyses.

Acknowledgments

We thank Tiffany Reese and Guoxun Wang for many helpful conversations about MNV egress, Kim Orth, Wei Peng, Katie Kang, David Heisler, Maarten De Jong for advice on protein purification and liposome assays, and Rob Orchard for advice on MNV experiments. We thank Andrea Erickson, Kim Orth, and Tiffany Reese for helpful comments on the manuscript.

This work was supported by NIH grants R37 AI074668 to J.K.P., T32 AI007520 to V.J.R.I, and T32AI005284 to R.W.M.

References

1. Burrell CJ, Howard CR, Murphy FA. (2017). Virus Replication. Fenner and White's Medical Virology.39-55.10.1016/b978-0-12-375156-0.00004-7

2. Domingo E, Holland JJ. (1997). RNA virus mutations and fitness for survival. Annu Rev Microbiol. 51:151-78.10.1146/annurev.micro.51.1.151
3. Bull RA, Tanaka MM, White PA. (2007). Norovirus recombination. J Gen Virol. 88(Pt 12):3347-59.10.1099/vir.0.83321-0
4. Furió V, Moya A, Sanjuán R. (2005). The cost of replication fidelity in an RNA virus. Proc Natl Acad Sci U S A. 102(29):10233-7.10.1073/pnas.0501062102
5. Bordería AV, Rozen-Gagnon K, Vignuzzi M. (2016). Fidelity Variants and RNA Quasispecies. Curr Top Microbiol Immunol. 392:303-22.10.1007/82_2015_483
6. Regoes RR, Hamblin S, Tanaka MM. (2013). Viral mutation rates: modelling the roles of within-host viral dynamics and the trade-off between replication fidelity and speed. Proc Biol Sci. 280(1750):20122047.10.1098/rspb.2012.2047
7. Dodd T, Botto M, Paul F, Fernandez-Leiro R, Lamers MH, Ivanov I. (2020). Polymerization and editing modes of a high-fidelity DNA polymerase are linked by a well-defined path. Nature Communications. 11(1):5379.10.1038/s41467-020-19165-2
8. Starr TN, Greaney AJ, Addetia A, Hannon WW, Choudhary MC, Dingens AS, et al. (2021). Prospective mapping of viral mutations that escape antibodies used to treat COVID-19. Science. 371(6531):850-4.doi:10.1126/science.abf9302
9. Wang Y, Pfeiffer JK. (2016). Emergence of a Large-Plaque Variant in Mice Infected with Coxsackievirus B3. mBio. 7(2):10.1128/mbio.00119-16.doi:10.1128/mbio.00119-16
10. Nguyen Y, Jesudhasan PR, Aguilera ER, Pfeiffer JK. (2019). Identification and Characterization of a Poliovirus Capsid Mutant with Enhanced Thermal Stability. J Virol. 93(6).10.1128/jvi.01510-18
11. Lanahan MR, Maples RW, Pfeiffer JK. (2021). Tradeoffs for a viral mutant with enhanced replication speed. Proc Natl Acad Sci U S A. 118(30).10.1073/pnas.2105288118
12. McFadden N, Bailey D, Carrara G, Benson A, Chaudhry Y, Shortland A, et al. (2011). Norovirus regulation of the innate immune response and apoptosis occurs via the product of the alternative open reading frame 4. PLoS Pathog. 7(12):e1002413.10.1371/journal.ppat.1002413
13. Karst SM, Wobus CE, Goodfellow IG, Green KY, Virgin HW. (2014). Advances in norovirus biology. Cell Host Microbe. 15(6):668-80.10.1016/j.chom.2014.05.015
14. Sosnovtsev SV, Belliot G, Chang KO, Prikhodko VG, Thackray LB, Wobus CE, et al. (2006). Cleavage map and proteolytic processing of the murine norovirus nonstructural polyprotein in infected cells. J Virol. 80(16):7816-31.10.1128/jvi.00532-06
15. Hyde JL, Sosnovtsev SV, Green KY, Wobus C, Virgin HW, Mackenzie JM. (2009). Mouse norovirus replication is associated with virus-induced vesicle clusters originating from membranes derived from the secretory pathway. J Virol. 83(19):9709-19.10.1128/jvi.00600-09
16. Cotton BT, Hyde JL, Sarvestani ST, Sosnovtsev SV, Green KY, White PA, et al. (2017). The Norovirus NS3 Protein Is a Dynamic Lipid- and Microtubule-Associated Protein Involved in Viral RNA Replication. Journal of Virology. 91(3):10.1128/jvi.02138-16.doi:10.1128/jvi.02138-16
17. Hyde JL, Mackenzie JM. (2010). Subcellular localization of the MNV-1 ORF1 proteins and their potential roles in the formation of the MNV-1 replication complex. Virology. 406(1):138-48.10.1016/j.virol.2010.06.047
18. Thackray LB, Wobus CE, Chachu KA, Liu B, Alegre ER, Henderson KS, et al. (2007). Murine Noroviruses Comprising a Single Genogroup Exhibit Biological Diversity despite Limited Sequence Divergence. Journal of Virology. 81(19):10460-73.doi:10.1128/jvi.00783-07
19. Karst SM, Wobus CE, Lay M, Davidson J, Virgin HWt. (2003). STAT1-dependent innate immunity to a Norwalk-like virus. Science. 299(5612):1575-8.10.1126/science.1077905
20. Hsu CC, Riley LK, Wills HM, Livingston RS. (2006). Persistent infection with and serologic cross-reactivity of three novel murine noroviruses. Comp Med. 56(4):247-51
21. Wobus CE, Karst SM, Thackray LB, Chang KO, Sosnovtsev SV, Belliot G, et al. (2004). Replication of Norovirus in cell culture reveals a tropism for dendritic cells and macrophages. PLoS Biol. 2(12):e432.10.1371/journal.pbio.0020432
22. Li T-F, Hosmillo M, Schwanke H, Shu T, Wang Z, Yin L, et al. (2018). Human Norovirus NS3 Has RNA Helicase and Chaperoning Activities. Journal of Virology. 92(5):10.1128/jvi.01606-17.doi:10.1128/jvi.01606-17
23. Han KR, Lee JH, Kotiguda GG, Jung KH, Chung MS, Kang S, et al. (2018). Nucleotide triphosphatase and RNA chaperone activities of murine norovirus NS3. J Gen Virol. 99(11):1482-93.10.1099/jgv.0.001151
24. Furman LM, Maaty WS, Petersen LK, Ettayebi K, Hardy ME, Bothner B. (2009). Cysteine protease activation and apoptosis in Murine norovirus infection. Virol J. 6:139.10.1186/1743-422x-6-139

25. Natoni A, Kass GEN, Carter MJ, Roberts LO. (2006). The mitochondrial pathway of apoptosis is triggered during feline calicivirus infection. J Gen Virol. 87(Pt 2):357-61.10.1099/vir.0.81399-0
26. Al-Molawi N, Beardmore VA, Carter MJ, Kass GEN, Roberts LO. (2003). Caspase-mediated cleavage of the feline calicivirus capsid protein. J Gen Virol. 84(Pt 5):1237-44.10.1099/vir.0.18840-0
27. ROBERTS LO, AL-MOLAWI N, CARTER MJ, KASS GEN. (2003). Apoptosis in Cultured Cells Infected with Feline Calicivirus. Annals of the New York Academy of Sciences. 1010(1):587-90.
28. Sosnovtsev SV, Prikhod'ko EA, Belliot G, Cohen JI, Green KY. (2003). Feline calicivirus replication induces apoptosis in cultured cells. Virus Res. 94(1):1-10.10.1016/s0168-1702(03)00115-1
29. Bok K, Prikhodko VG, Green KY, Sosnovtsev SV. (2009). Apoptosis in murine norovirus-infected RAW264.7 cells is associated with downregulation of survivin. J Virol. 83(8):3647-56.10.1128/jvi.02028-08
30. Dubois H, Sorgeloos F, Sarvestani ST, Martens L, Saeys Y, Mackenzie JM, et al. (2019). Nlrp3 inflammasome activation and Gasdermin D-driven pyroptosis are immunopathogenic upon gastrointestinal norovirus infection. PLoS Pathog. 15(4):e1007709.10.1371/journal.ppat.1007709
31. Wang G, Zhang D, Orchard RC, Hancks DC, Reese TA. (2023). Norovirus MLKL-like protein initiates cell death to induce viral egress. Nature. 616(7955):152-8.10.1038/s41586-023-05851-w
32. Aktepe TE, Deerain JM, Hyde JL, Fritzlar S, Mead EM, Carrera Montoya J, et al. (2024). Norovirus-mediated translation repression promotes macrophage cell death. PLoS Pathog. 20(9):e1012480.10.1371/journal.ppat.1012480
33. Bock FJ, Tait SWG. (2020). Mitochondria as multifaceted regulators of cell death. Nature Reviews Molecular Cell Biology. 21(2):85-100.10.1038/s41580-019-0173-8
34. Arias A, Bailey D, Chaudhry Y, Goodfellow I. (2012). Development of a reverse-genetics system for murine norovirus 3: long-term persistence occurs in the caecum and colon. J Gen Virol. 93(Pt 7):1432-41.10.1099/vir.0.042176-0
35. Budicini MR, Rodriguez-Irizarry VJ, Maples RW, Pfeiffer JK. (2024). Murine norovirus mutants adapted to replicate in human cells reveal a post-entry restriction. J Virol. 98(5):e0004724.10.1128/jvi.00047-24
36. Chu CT, Ji J, Dagda RK, Jiang JF, Tyurina YY, Kapralov AA, et al. (2013). Cardiolipin externalization to the outer mitochondrial membrane acts as an elimination signal for mitophagy in neuronal cells. Nat Cell Biol. 15(10):1197-205.10.1038/ncb2837
37. Liu J, Epand RF, Durrant D, Grossman D, Chi NW, Epand RM, et al. (2008). Role of phospholipid scramblase 3 in the regulation of tumor necrosis factor-alpha-induced apoptosis. Biochemistry. 47(15):4518-29.10.1021/bi701962c
38. Ryan T, Bamm VV, Stykel MG, Coackley CL, Humphries KM, Jamieson-Williams R, et al. (2018). Cardiolipin exposure on the outer mitochondrial membrane modulates α-synuclein. Nature Communications. 9(1):817.10.1038/s41467-018-03241-9
39. Kahan SM, Liu G, Reinhard MK, Hsu CC, Livingston RS, Karst SM. (2011). Comparative murine norovirus studies reveal a lack of correlation between intestinal virus titers and enteric pathology. Virology. 421(2):202-10.
40. Sharon AJ, Filyk HA, Fonseca NM, Simister RL, Filler RB, Yuen W, et al. (2022). Restriction of Viral Replication, Rather than T Cell Immunopathology, Drives Lethality in Murine Norovirus CR6-Infected STAT1-Deficient Mice. J Virol. 96(6):e0206521.10.1128/jvi.02065-21
41. Roth AN, Helm EW, Mirabelli C, Kirsche E, Smith JC, Eurell LB, et al. (2020). Norovirus infection causes acute self-resolving diarrhea in wild-type neonatal mice. Nature Communications. 11(1):2968.10.1038/s41467-020-16798-1
42. Pfister T, Wimmer E. (2001). Polypeptide p41 of a Norwalk-like virus is a nucleic acid-independent nucleoside triphosphatase. J Virol. 75(4):1611-9.10.1128/jvi.75.4.1611-1619.2001
43. Deerain JM, Aktepe TE, Trenerry AM, Ebert G, Hyde JL, Charry K, et al. (2024). Murine norovirus infection of macrophages induces intrinsic apoptosis as the major form of programmed cell death. Virology. 589:109921.
44. Yen JB, Chen LW, Wei LH, Hung CH, Wang SS, Lin CL, et al. (2021). Identification and Characterization of Human Norovirus NTPase Regions Required for Lipid Droplet Localization, Cellular Apoptosis, and Interaction with the Viral P22 Protein. Microbiol Spectr. 9(1):e0042221.10.1128/Spectrum.00422-21
45. Doerflinger SY, Cortese M, Romero-Brey I, Menne Z, Tubiana T, Schenk C, et al. (2017). Membrane alterations induced by nonstructural proteins of human norovirus. PLoS Pathog. 13(10):e1006705.10.1371/journal.ppat.1006705

46. Murphy JM, Czabotar PE, Hildebrand JM, Lucet IS, Zhang JG, Alvarez-Diaz S, et al. (2013). The pseudokinase MLKL mediates necroptosis via a molecular switch mechanism. Immunity. 39(3):443-53.10.1016/j.immuni.2013.06.018
47. Sun L, Wang H, Wang Z, He S, Chen S, Liao D, et al. (2012). Mixed Lineage Kinase Domain-like Protein Mediates Necrosis Signaling Downstream of RIP3 Kinase. Cell. 148(1):213-27.
48. Tanzer MC, Tripaydonis A, Webb AI, Young SN, Varghese LN, Hall C, et al. (2015). Necroptosis signalling is tuned by phosphorylation of MLKL residues outside the pseudokinase domain activation loop. Biochem J. 471(2):255-65.10.1042/bj20150678
49. Amand HL, Fant K, Nordén B, Esbjörner EK. (2008). Stimulated endocytosis in penetratin uptake: effect of arginine and lysine. Biochem Biophys Res Commun. 371(4):621-5.10.1016/j.bbrc.2008.04.039
50. Wender PA, Mitchell DJ, Pattabiraman K, Pelkey ET, Steinman L, Rothbard JB. (2000). The design, synthesis, and evaluation of molecules that enable or enhance cellular uptake: peptoid molecular transporters. Proc Natl Acad Sci U S A. 97(24):13003-8.10.1073/pnas.97.24.13003
51. Hwang S, Alhatlani B, Arias A, Caddy SL, Christodoulou C, Cunha JB, et al. (2014). Murine norovirus: propagation, quantification, and genetic manipulation. Curr Protoc Microbiol. 33:15k.2.1-61.10.1002/9780471729259.mc15k02s33

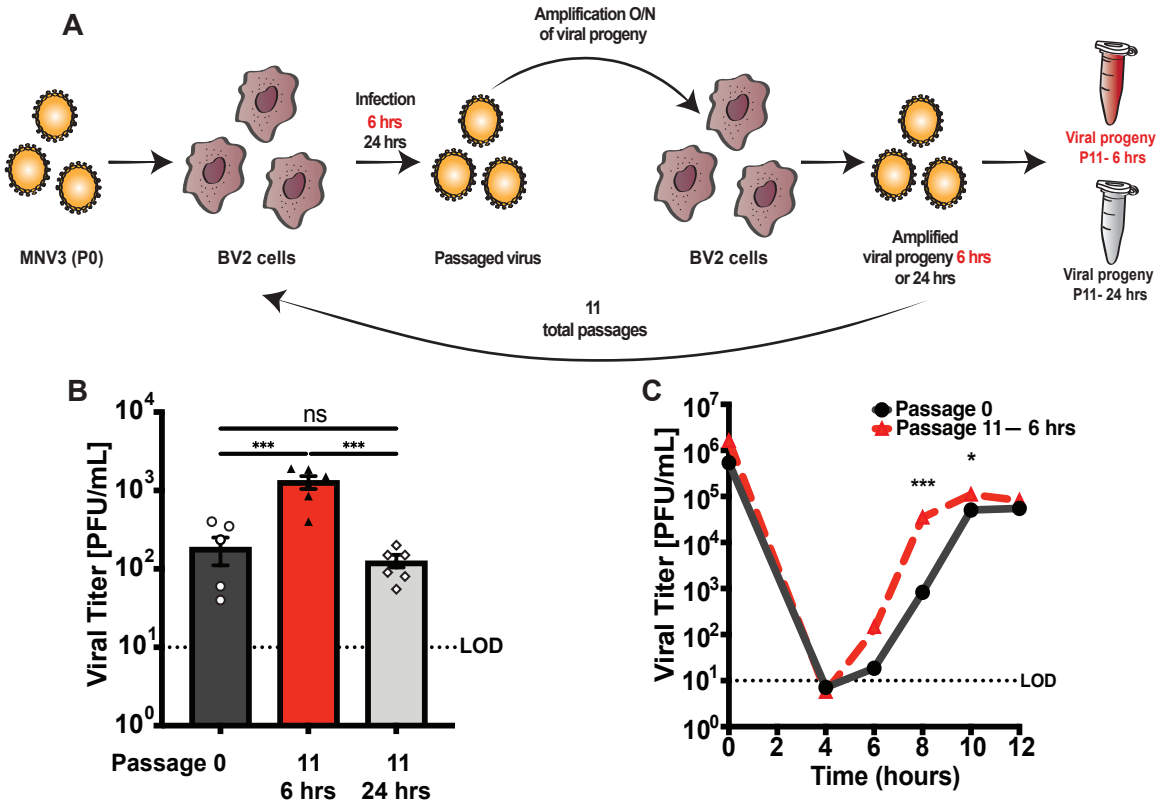

Figure 1. Selection to enrich for fast-replicating MNV mutants. (A) Schematic showing serial passage strategy. Initial MNV3 stock (P0) was used to infect BV2 cells, and progeny were harvested at 6 hours or 24 hours post-infection. Low titer viral progeny harvested at 6 hours were amplified overnight in BV2 cells to facilitate subsequent passages. Half of the volume of each sample was used to initiate a new passage, and the cycle was repeated 11 times. (B) Viral infection assay comparing the initial stock virus (Passage 0) and viruses passaged 11 times, collecting at 6 hours vs. 24 hours. BV2 cells were infected at an MOI of 0.1 for 6 hours. Cells and supernatant were pooled for each sample, and viral titers were quantified via plaque assay. Data are mean ± SEM (n=6, ≥ 3 independent experiments). *P<0.05, one-way ANOVA. (C) Single-cycle growth curve of Passage 0 and Passage 11-6 hrs . BV2 cells were infected at MOI 0.1 and cells and supernatant were collected and viral titer determined via plaque assay. Data are mean ± SEM (n=7, ≥ 3 independent experiments). *P<0.05, unpaired *t* test. LOD, limit of detection.

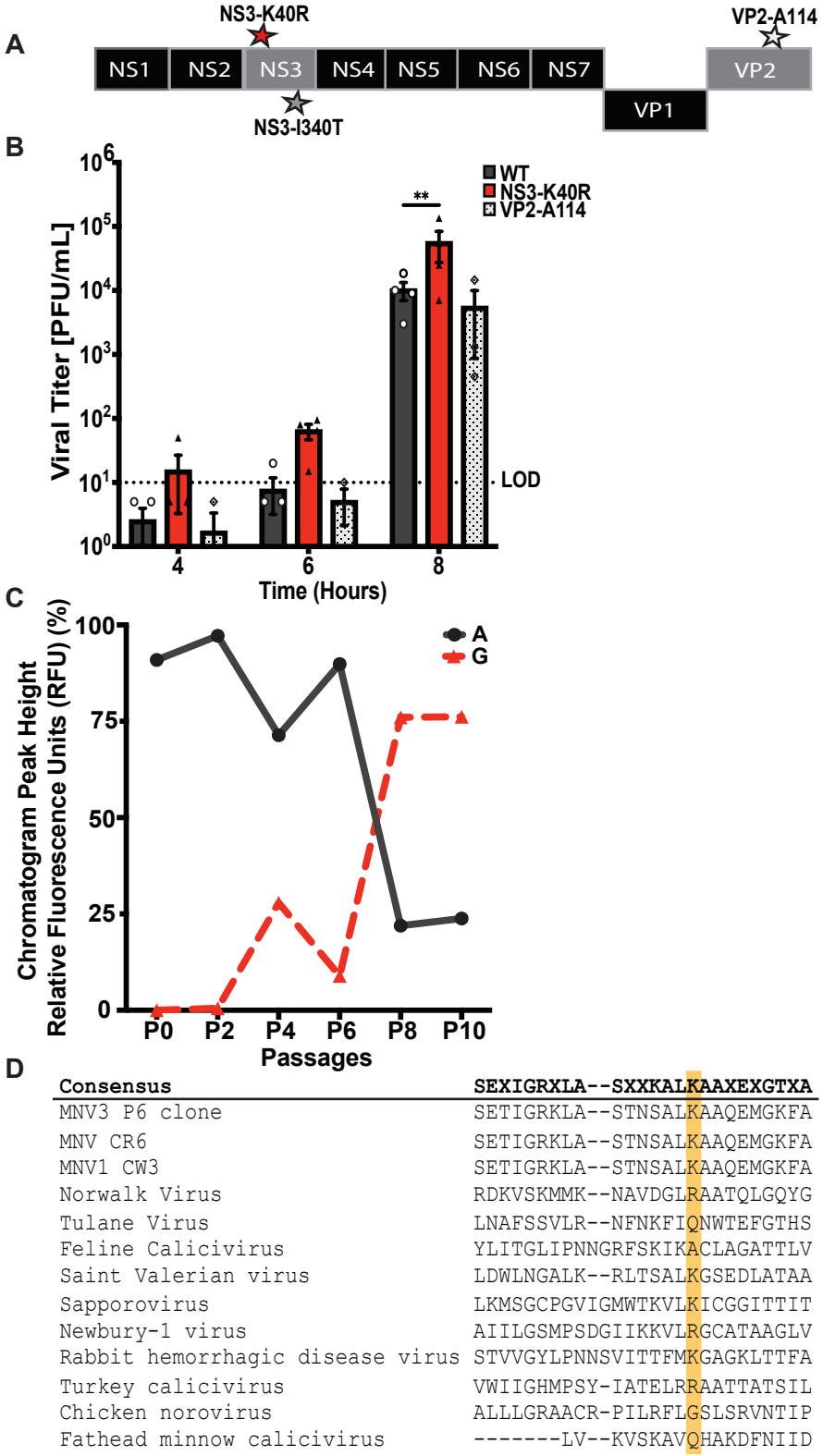

Figure 2. NS3-K40R is sufficient for the faster MNV3 replication phenotype. (A) Schematic of MNV3 genome with mutations found after eleven passages. Consensus sequence analysis revealed three mutations in viral progeny from passage 11-6 hr stocks: Two amino acid substitutions in NS3, K40R and I340T, and a silent mutation in the minor capsid protein VP2. Passage 11-24 hr stocks also contained the NS3-I340T mutation. (B) Viral infection assay of MNV3 WT, NS3-K40R and VP2-114. Infectious clone-derived viruses bearing NS3-K40R, the VP2-114 silent mutation, or no engineered mutations (WT) were used to infect BV2 cells at an MOI 0.1. Cells and supernatant were collected, and virus was quantified via plaque assay. Data are presented as mean ± SEM ($n \leq 4$; ≥ 4 independent experiments). *$P<0.05$, two-way ANOVA. (C) Emergence of adenine to guanine (AAG to AGG) mutation at position 1147 (NS3 amino acid 40) during viral passaging. The substitution of adenine with guanine changed coding from lysine to arginine. Peak heights were determined from chromatograms of the consensus sequence across passages. The percentages of peak heights were calculated based on the relative abundance of all four nucleotides at position 1147. (D) Conservation of amino acids at position 25 to 49 of NS3 across selected caliciviruses. Viruses are arranged based on their percentage identity relative to MNV3. Amino acid sequence alignment was performed using MUSCLE. Lysine 40 (K40) of NS3 is marked with a yellow rectangle. LOD, limit of detection.

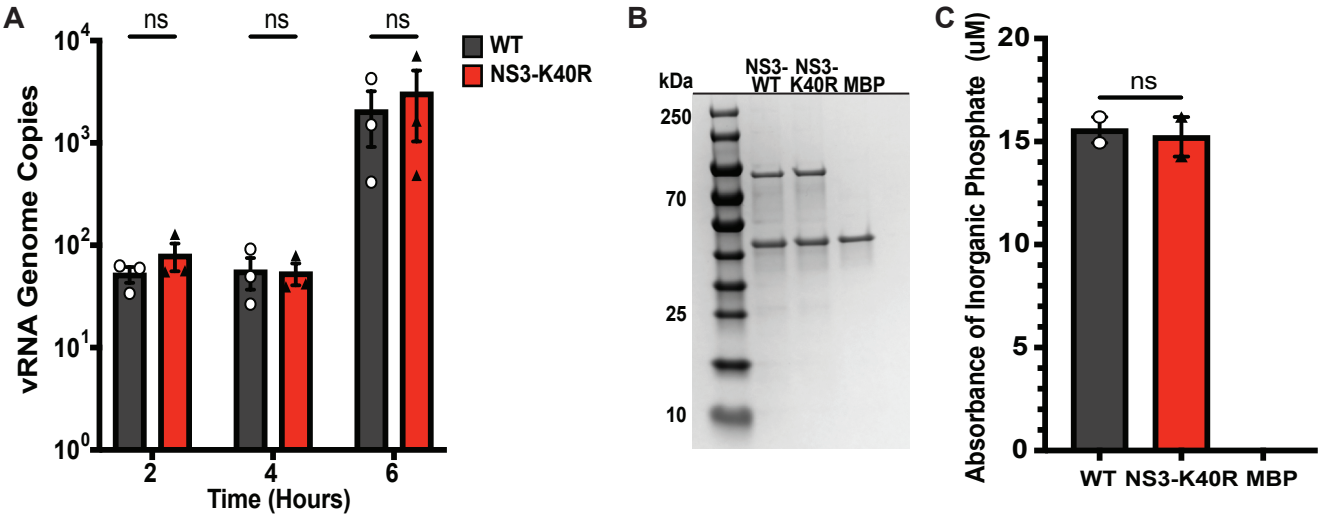

Figure 3. NS3 K40R does not alter RNA synthesis or NTPase activity. (A) Quantification of viral RNA during infection. BV2 cells were infected with WT or NS3-K40R at MOI 2, and viral RNA at indicated time points was harvested and quantified via RT-qPCR targeting MNV ORF1. Data are mean ± SEM (n=3, ≥ 3 independent experiments). *P<0.05, two-way ANOVA (B) Purified MBP-NS3 proteins used for NTPase assay. MBP-NS3 fusion proteins or MBP protein alone were purified and analyzed by 4–20% SDS-PAGE, followed by Coomassie Blue staining. The bands of proteins were quantified using ImageJ. (C) NTPase activity of purified NS3 proteins. NS3-MBP fusion proteins or MBP protein alone were incubated with 10 μM ATP for 30 min at 37°C, and inorganic phosphate released from ATP hydrolysis was quantified via a colorimetric assay. Data are mean ± SEM (Representative data from three independent protein preparations). *P<0.05, ANOVA.

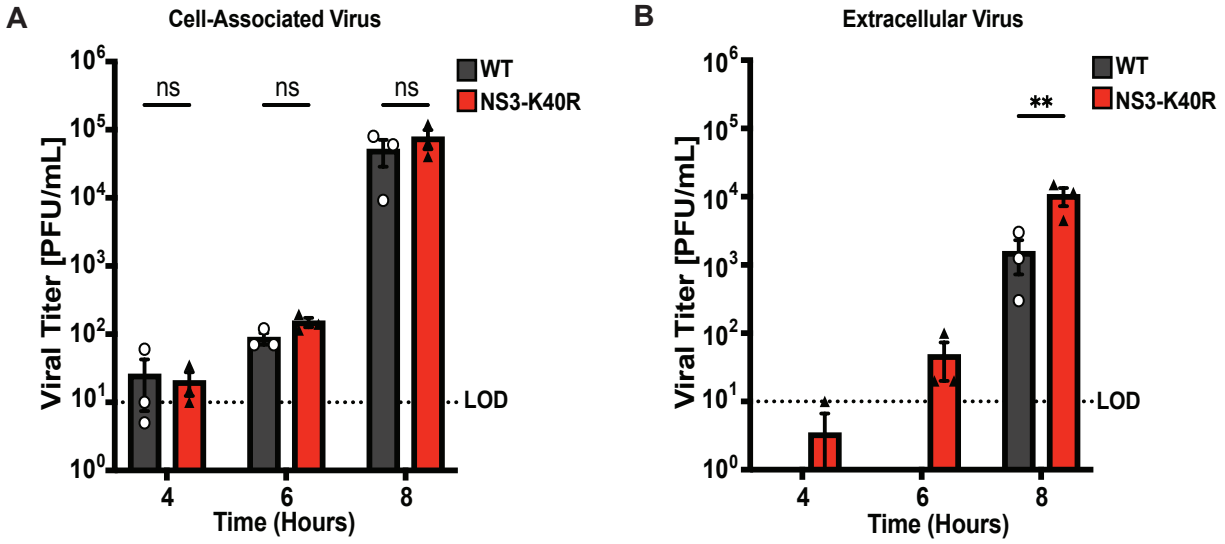

Figure 4. NS3-K40R increases extracellular viral titers but not cell-associated viral titers. BV2 cells were infected with MNV3 WT or NS3-K40R at MOI 0.1 for 4, 6 and 8 hrs post-infection, and progeny were harvested from (A) cells (representing virion particles within cells) or (B) culture supernatants (representing extracellular virus) followed by plaque assay quantification. Data are mean ± SEM (n=3, ≥ 3 independent experiments). *P<0.05, two-way ANOVA. LOD, limit of detection.

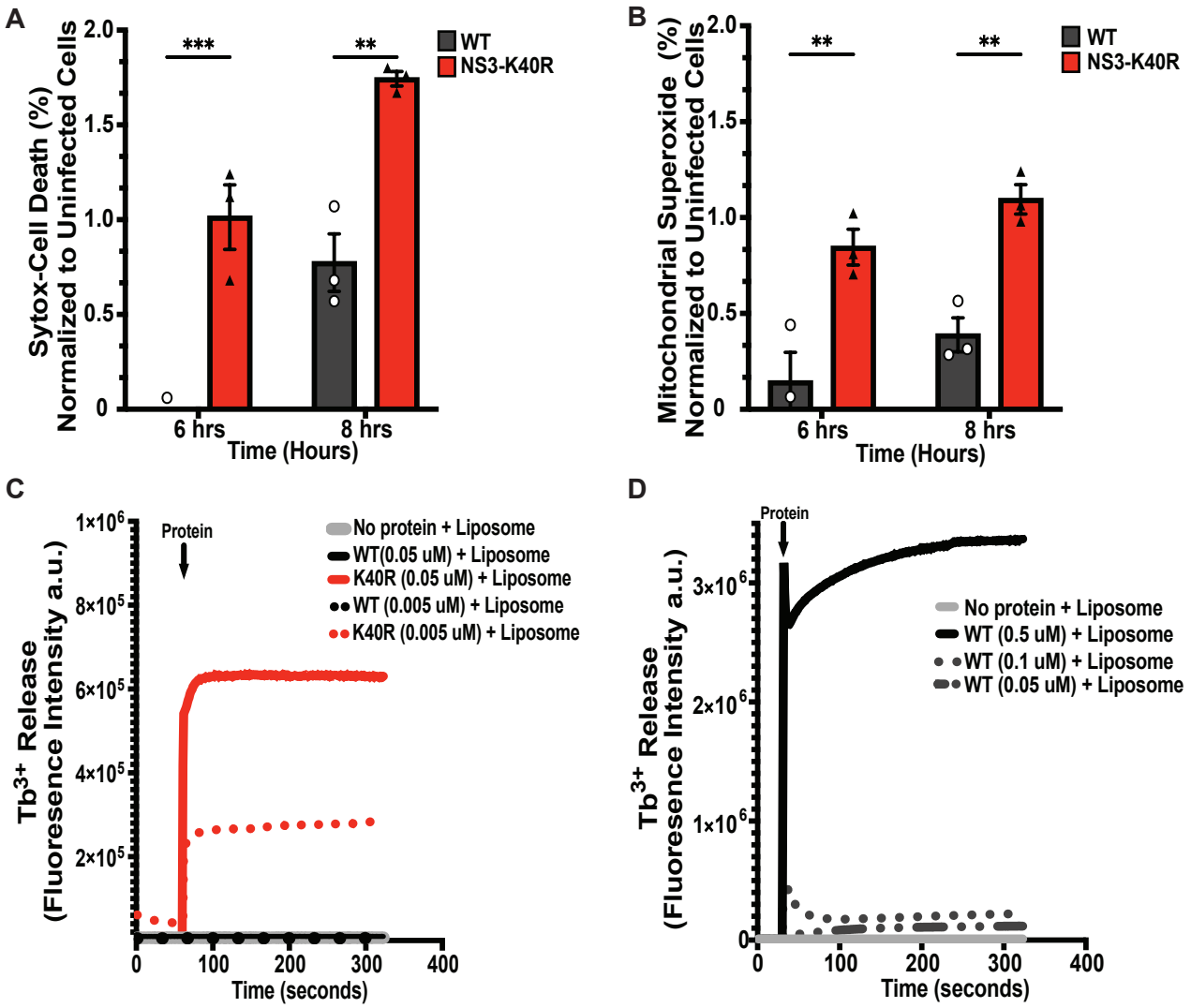

Figure 5. NS3-K40R induces increased cell death, mitochondrial dysfunction, and membrane disruption. (A) NS3-K40R increases cell death at early times post-infection. BV2 cells were infected with WT or NS3-K40R at MOI 2 and at 6 or 8 hours post-infection the number of dead cells was quantified by flow cytometry to detect Sytox nucleic acid staining of non-viable cells. Values represent the subtraction of the percentage of mock-treated cells. Data are mean ± SEM (n=3, ≥ 3 independent experiments). *P<0.05, two-way ANOVA. (B) NS3-K40R increases mitochondrial superoxide at early times post-infection. BV2 cells were infected with WT or NS3-K40R at MOI 2 and at 6 or 8 hours post-infection mitochondrial superoxide was quantified by flow cytometry to detect MitoSOX staining. Values represent the subtraction of the percentage of mock-treated cells. Data are mean ± SEM (n=3, ≥ 3 independent experiments). *P<0.05, two-way ANOVA. (C-D) Cardiolipin liposome leakage assays with purified-tagless NS3 proteins. (C) Liposome leakage assay with low concentrations of NS3 proteins reveals increased activity of NS3-K40R compared with NS3-WT. Cardiolipin liposomes (0.1 mM; 80% phosphatidylcholine, 20% cardiolipin) were incubated with purified NS3-WT and NS3-K40R proteins at 0.05 μM and 0.005 μM and Tb^{3+} fluorescence leakage was quantified upon binding to dipicolinic acid (DPA). Data are representative of two independent experiments with separate protein/liposome preparations. (D) NS3-WT protein induces liposome leakage at high protein concentrations. After the experiment in panel C, the assay was repeated using higher concentrations of NS3-WT protein (0.5 μM, 0.1 μM, and 0.05 μM). a.u., arbitrary units.

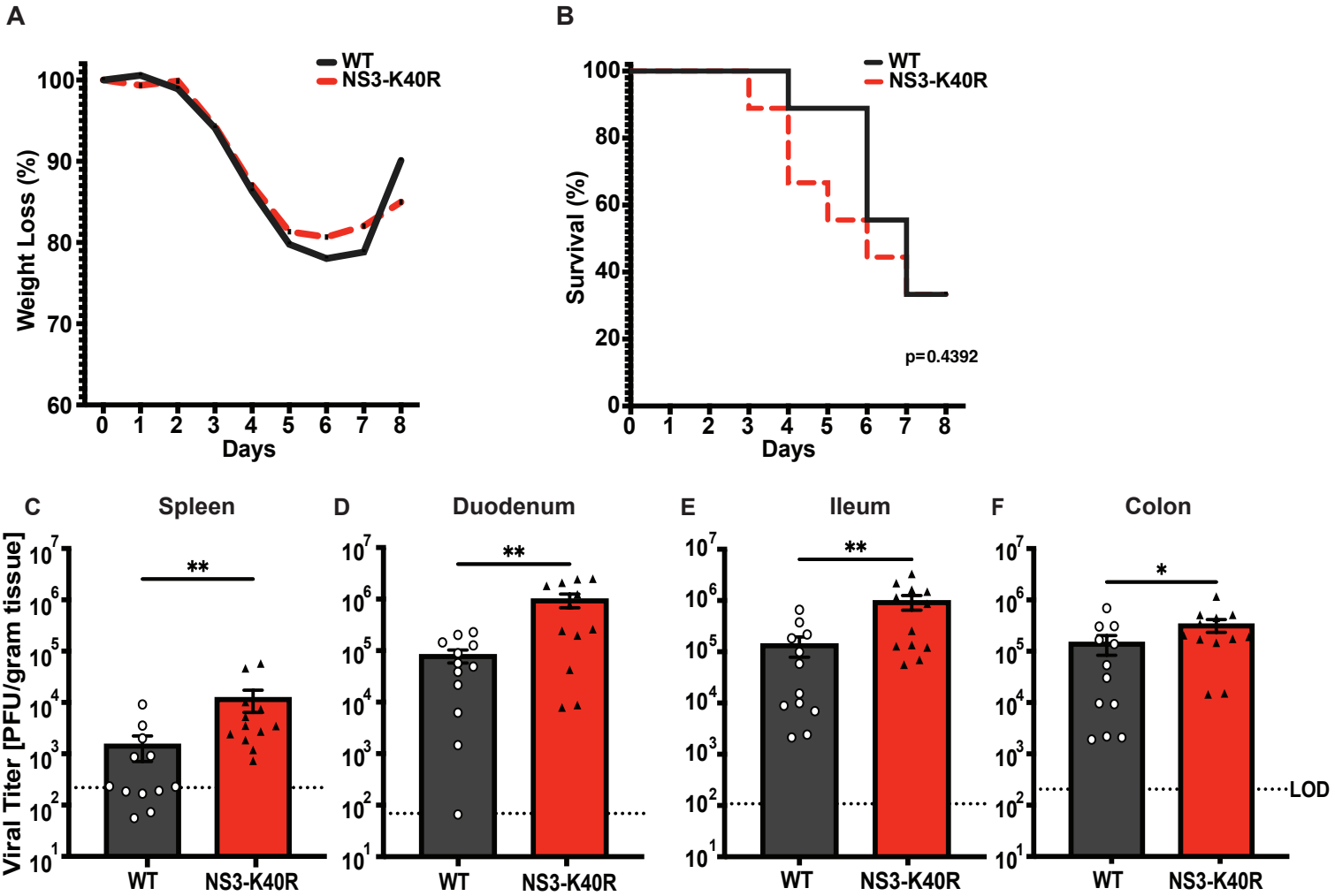

Figure 6. NS3-K40R increases viral titers in *STAT1* $^{-/-}$ mice.
STAT1$^{-/-}$ mice were perorally infected with 10^6 PFU of WT and NS3-K40R followed by assessment of (A) weight loss, (B) survival until 8 days post-infection. Data are mean ± SEM (n=8, ≥ 2 independent experiments). *P<0.05, Mantel-Cox test. Infections were repeated, but mice were sacrificed at 24 hours post-infection for viral titer analysis via plaque assay for tissues including (C) spleen, (D) duodenum, (E) ileum, and (F) colon. Data are mean ± SEM (n=12, ≥2 independent experiments). *P<0.05, unpaired *t* test. LOD, limit of detection. LOD was determined based on the average tissue weight.

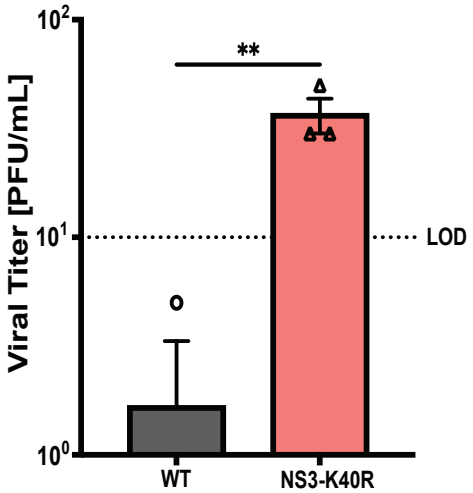

Supplemental Figure 1. NS3-K40R increases viral titer in the supernatant of RAW cells at an early time point post-infection. RAW264.7 cells were infected with WT and NS3-K40R at MOI 0.1 for 8 hours. Extracellular virus was measured via plaque assay. Data are mean ± SEM (n=3, ≥ 3 independent experiments). *P<0.05, unpaired t test. LOD, limit of detection.

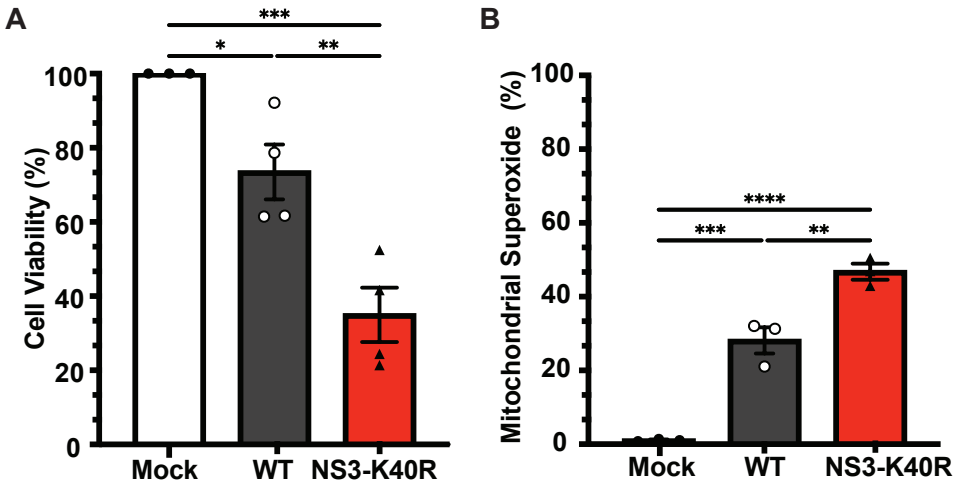

Supplemental Figure 2. MNV3 NS3-K40R induces increased cell death and mitochondrial dysfunction late in infection. (A) NS3-K40R increases cell death at 24 hrs post-infection. BV2 cells were infected with WT or NS3-K40R at MOI 2 and at 24 hours post-infection cell viability was quantified using ATP-based assay. Data are mean ± SEM (n=4, ≥ 3 independent experiments). *P<0.05, one-way ANOVA. (B) NS3-K40R increases mitochondrial superoxide at 24 hrs post-infection. BV2 cells were infected with WT or NS3-K40R at MOI 2 and at 24 hours post-infection mitochondrial superoxide was quantified by flow cytometry to detect MitoSOX staining. Data are mean ± SEM (n=3, ≥ 3 independent experiments). *P<0.05, one-way ANOVA.

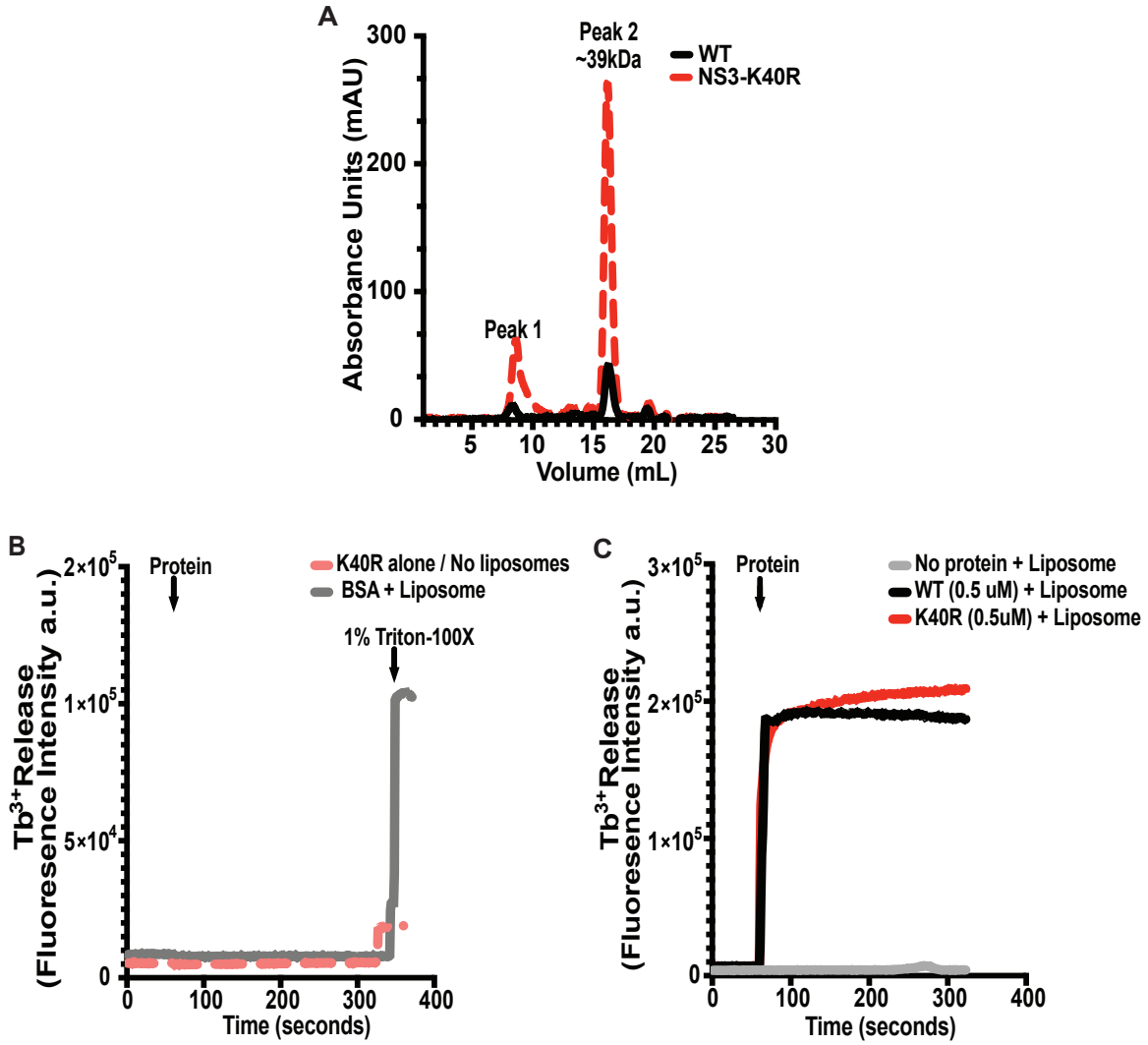

Supplemental Figure 3. NS3 protein preparation and controls for the liposome leakage assays. (A) Purification of tagless NS3 proteins for liposome leakage assays. Purified His6-MBP-NS3 fusion proteins were treated with TEV protease to remove the His6-MBP tag. Following cleavage, the proteins were purified using Ni-NTA resin and subjected to size-exclusion chromatography. Absorbance peaks from size-exclusion chromatography are shown (NS3-WT in black and NS3-K40R in red) and the peak at approximately 16–17 mL was collected for use in liposome leakage assays. (B and C) Controls for the liposome leakage assay. (B) NS3-K40R was incubated in the absence of liposomes, or 0.5 μM BSA was incubated with cardiolipin liposomes (0.1 mM; 80% phosphatidylcholine and 20% cardiolipin) and at the end of the experiment detergent was added to disrupt liposomes. The leakage of Tb^{3+} fluorescence leakage was quantified upon binding to dipicolinic acid (DPA). Data are representative of two independent experiments. (C) Experiment was repeated as in B, but cardiolipin liposomes (0.1 mM; 80% phosphatidylcholine and 20% cardiolipin) were incubated with purified NS3-WT and NS3-K40R proteins at 0.5 μM or no protein, and leakage of Tb^{3+} fluorescence leakage was quantified upon binding to DPA. Data are representative of two independent experiments with separate protein/liposome preparations. a.u.,arbitrary units.